

# Fast procedure for Non-uniform optimum design of stiffened shells under buckling constraint

Peng Hao<sup>1</sup> · Bo Wang<sup>1</sup> · Kuo Tian<sup>1</sup> · Gang Li<sup>1</sup> · Yu Sun<sup>1</sup> · Chunxiao Zhou<sup>2</sup>

Received: 25 October 2015 / Revised: 27 June 2016 / Accepted: 9 September 2016 / Published online: 22 September 2016  
© Springer-Verlag Berlin Heidelberg 2016

**Abstract** For tailoring the non-uniform axial compression, each sub-panel of stiffened shells should be designed separately to achieve a high load-carrying efficiency. Motivated by the challenge caused by numerous variables and high computational cost, a fast procedure for the minimum weight design of non-uniform stiffened shells under buckling constraint is proposed, which decomposes a hyper multi-dimensional problem into a hierarchical optimization with two levels. To facilitate the post-buckling optimization, an efficient equivalent analysis model of stiffened shells is developed based on the Numerical Implementation of Asymptotic Homogenization Method. In particular, the effects of non-uniform load, internal pressure and geometric imperfections are taken into account during the optimization. Finally, a typical fuel tank of launch vehicle is utilized to demonstrate the effectiveness of the proposed procedure, and detailed comparison with other optimization methodologies is made.

**Keyword** Non-uniform stiffened shell · Buckling · Equivalent model · Fast procedure · Hierarchical optimization

---

✉ Bo Wang  
wangbo@dlut.edu.cn

<sup>1</sup> State Key Laboratory of Structural Analysis for Industrial Equipment, Department of Engineering Mechanics, Dalian University of Technology, Dalian 116023, China

<sup>2</sup> Beijing Institute of Astronautical Systems Engineering, Beijing 100076, China

## 1 Introduction

During the flight condition of launch vehicles, stiffened shells in the boosters would suffer from a non-uniform axial compression along circumferential direction, as shown in Fig. 1. As is well known, stiffened shells under axial compression are prone to buckling and collapse (Degenhardt et al. 2008; Loughlan 1994), and their load-carrying capacities are very sensitive to geometric imperfections (Paulo et al. 2013; Hao et al. 2015a). The design of stiffened shells under non-uniform axial compression is very complicated, since the buckling behavior is prominently characterized by geometric nonlinearity due to the coupling effects of axial compression and additional bending loads, as well as initial imperfections.

In the previous works, an exhaustive study of imperfection sensitivity analyses has been conducted for cylindrical shells under axial compression with the goal of determining the knockdown effect with more accuracy (Hilburger et al. 2006; Castro et al. 2014; Wang et al. 2014; Degenhardt et al. 2014; Godoy et al. 2015; Azarboni et al. 2015; Friedrich et al. 2015; Wang and Croll 2015; Liang et al. 2015). Since the buckling behavior of thin-walled structures with geometric imperfections is very complicated, high-fidelity post-buckling analysis procedure becomes more popular for the imperfection sensitivity analysis and design optimization of stiffened shells. Up to now, eigenmode-shape imperfection was commonly used in the load-carrying capacity assessment of thin-walled structures, because it represents the deformation shapes with a high bias towards buckling (Teng and Song 2001; Hao et al. 2013).

With the growing application of stiffened shells in future launch vehicles, structural weight becomes increasingly more important for lifting payload. Therefore, many optimizations have been conducted in previous studies. Typically, the minimum weight design optimization of stiffened panels was

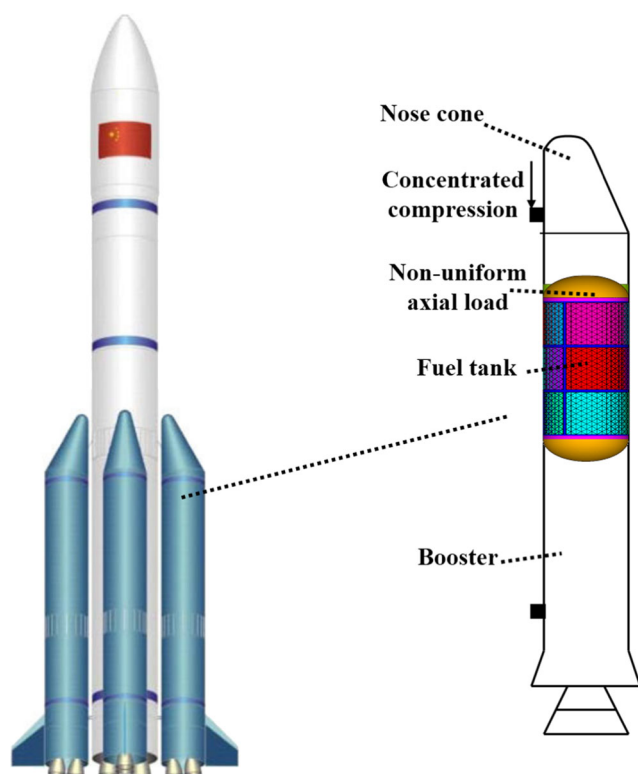


**Fig. 1** Stiffened shells subjected to non-uniform load in launch vehicles

carried out based on PANDA2 and validated by STAGS (Bushnell and Bushnell 1994). Also, the buckling, strength and displacement constraints were considered by Starnes Jr and Haftka (1979). The optimization and antioptimization of composite cylindrical shells based on measured imperfections were conducted by Elishakoff et al. (2012). Foryś (2015) performed the optimization of stiffened shells using the modified particle swarm optimization method. Recently, the optimization of composite panels considering worst shape imperfections was performed by Henrichsen et al. (2015). In addition, the crack propagation was also taken into account in the design of composite stiffened panels (Vitali et al. 2002). Since nonlinear post-buckling analysis of stiffened shells is generally time-consuming, the availability of a fast analysis method indeed represents a crucial aspect to move from a more costly optimization to a faster optimization loop. Therefore, Smeared Stiffener Method (SSM) in conjunction with the Rayleigh-Ritz method were utilized to calculate the buckling load of stiffened shells in the preliminary design phase (Lamberti et al. 2003). Then, a bi-step procedure for post-buckling analysis of stiffened panels was developed based on the energy principle and the Rayleigh-Ritz method (Vescovini and Bisagni 2013). Fukunaga and Vanderplaats (1991) carried out the buckling optimization of composite shells using lamination parameters, and then solved the inverse problem to obtain explicit lamination sequences. Moreover, Hao et al. (2014) proposed a hybrid optimization framework of stiffened

shells by combining the efficiency of SSM with the accuracy of FEM, and then a hybrid reliability-based design optimization framework was established based on SSM and FEM (Hao et al. 2015b). Compared to the SSM, the asymptotic homogenization (AH) method has a higher prediction accuracy of effective stiffness for periodic structures, which is derived based on a rigorous mathematical foundation (Kalamkarov et al. 2009). However, the AH method is difficult to be implemented numerically, which severely limits its applications. Motivated by this difficulty, Cheng et al. (2013) and Cai et al. (2014) established a novel numerical implementation of the asymptotic homogenization (NIAH) method for periodic plates. Furthermore, Wang et al. (2015) developed a hybrid analysis and optimization framework for hierarchical stiffened plates based on the NIAH method. However, small deflection assumption was made in the previous studies, and geometric nonlinearity was not taken into account, which would significantly affect the post-buckling behavior of stiffened shells. To this end, Hao et al. (2016a) proposed an efficient optimization framework of curvilinearly stiffened shells by utilization of the NIAH method, where the effect of large deflection was considered. As a supplement of current theory, Meziane et al. (2014) developed a simple higher order shear and normal deformation theory to improve the efficiency and accuracy of buckling analysis. However, with regard to the design of fuel tank in the boosters of launch vehicle, the non-uniform compression and internal pressure should be considered simultaneously for stiffened shells. Obviously, the complex load conditions put forward a higher accuracy requirement for the equivalent stiffness coefficients of equivalent model, especially for the coupling stiffness coefficients.

In addition, there is only limited work on the analysis and optimization of stiffened shells under non-uniform axial compression in the available literatures. As was stated by Greenberg and Stavsky (1995), the buckling response of composite cylindrical shells under circumferentially non-uniform axial loads was studied. Also, the buckling behavior of composite panels subjected to non-uniform loads was investigated by Soni et al. (2013). Ovesy and Fazilati (2014) investigated the dynamic buckling behavior of composite panels under non-uniform in-plane load. Since non-uniform stiffened shell usually involves a wide range of parameters associated with a complex buckling behavior, the design of such structures requires sophisticated analysis and optimization techniques. Hierarchical optimization is also a good choice for such a complex problem. The global/local design optimization of large wing structures was performed by Ragon et al. (1997). Carrera et al. (2003) carried out the optimization of space vehicles by a novel bi-level optimization procedure. Peeters et al. (2015) presented a multi-level approach to reduce the required number of FE analyses in the optimization of variable stiffness laminates. Another example is the work by Hao et al. (2012) who proposed a surrogate-based optimization

framework with adaptive sampling for stiffened panels subjected to non-uniform load, where stiffener dimensions (rather than stiffener types) can be different in each sub-panel.

Motivated by these previous studies, a fast procedure for non-uniform optimum design of stiffened shells under buckling constraint is proposed in this study, whose major contribution lies in the utilization of equivalent analysis model and hierarchical optimization methodology. This paper is organized as follows. A brief introduction of NIAH method is given in Section 2. Then, the fast optimization procedure is proposed in Section 3, and the proposed hierarchical optimization framework is validated by a simple benchmark example. To reduce the computational burden of post-buckling analysis, an efficient equivalent model of fuel tank in launch vehicles is developed based on the NIAH method in Section 4. Different from the previous studies, the effects of non-uniform load, internal pressure, as well as geometric imperfections are considered simultaneously herein. After that, the non-uniform optimum design of the illustrative example is obtained by the proposed procedure. Finally, detailed comparisons with current design methods are made from the point-of-view of computational efficiency and weight reduction.

## 2 Numerical implementation of asymptotic homogenization (NIAH) method

To fully explore the potential of load-carrying capacity, stiffened shells usually serve in nonlinear post-buckling regime until global collapse occurs. For this reason, the explicit dynamic analysis method should be employed to solve the problem of convergence. As mentioned earlier, since nonlinear post-buckling analysis of stiffened shells based on the explicit dynamic method is generally time-consuming, global optimization of stiffened shells based on detailed FE models is almost not affordable. For this reason, the NIAH method is adopted in this study to release the computational burden.

For the traditional implementation of AH method, the effective stiffness coefficients  $A_{ij}$ ,  $B_{ij}$  and  $D_{ij}$  of the periodic unit cell  $\Omega$  can be obtained as

$$\begin{aligned} \mathbf{A}_{ij} &= \frac{1}{|\Omega|} \int_{\Omega} (\boldsymbol{\varepsilon}_i^0 - \boldsymbol{\varepsilon}_i^*)^T \mathbf{c} (\boldsymbol{\varepsilon}_j^0 - \boldsymbol{\varepsilon}_j^*) d\Omega \\ \mathbf{B}_{ij} &= \frac{1}{|\Omega|} \int_{\Omega} (\boldsymbol{\varepsilon}_i^0 - \boldsymbol{\varepsilon}_i^*)^T \mathbf{c} \begin{pmatrix} 0 \\ \bar{\boldsymbol{\varepsilon}}_j^0 - \bar{\boldsymbol{\varepsilon}}_j^* \end{pmatrix} d\Omega \\ \mathbf{D}_{ij} &= \frac{1}{|\Omega|} \int_{\Omega} \begin{pmatrix} 0 \\ \bar{\boldsymbol{\varepsilon}}_i^0 - \bar{\boldsymbol{\varepsilon}}_i^* \end{pmatrix}^T \mathbf{c} \begin{pmatrix} 0 \\ \bar{\boldsymbol{\varepsilon}}_j^0 - \bar{\boldsymbol{\varepsilon}}_j^* \end{pmatrix} d\Omega \end{aligned} \tag{1}$$

where  $c$  is the elasticity matrix, the superscripts  $i$  and  $j$  denote the load cases ( $i, j \in \{1, 2, 6\}$ ). The unit strain fields contain three in-plane strain fields  $\boldsymbol{\varepsilon}_i^0$  and three flexural strain fields  $\bar{\boldsymbol{\varepsilon}}_i^0$ , and the characteristic strain fields include three in-plane strain fields  $\boldsymbol{\varepsilon}_i^*$  and three flexural strain fields  $\bar{\boldsymbol{\varepsilon}}_i^*$ . For the AH

method, a unit strain field is required in solving the cell equation, which cannot be easily obtained from the FEM method. The formula derivation and numerical implementation of the NIAH method can be summarized in Fig. 2.

Firstly, the unit strain fields  $\boldsymbol{\varepsilon}_i^0$  and  $\bar{\boldsymbol{\varepsilon}}_i^0$  can be expressed by the corresponding nodal displacement fields  $\boldsymbol{\chi}_i^0$  and  $\bar{\boldsymbol{\chi}}_i^0$  with strain–displacement matrix  $B$

$$\begin{aligned} \boldsymbol{\varepsilon}_i^0 &= \mathbf{B}\boldsymbol{\chi}_i^0 \\ \bar{\boldsymbol{\varepsilon}}_i^0 &= \mathbf{B}\bar{\boldsymbol{\chi}}_i^0 \end{aligned} \tag{2}$$

Then, the FE model of the structure cell is established, and the nodal displacement fields  $\boldsymbol{\chi}_i^0$  and  $\bar{\boldsymbol{\chi}}_i^0$  are applied to the FE model. By performing the first static analysis, the reaction nodal force vectors  $\mathbf{f}_i$  and  $\bar{\mathbf{f}}_i$  are obtained as follows

$$\begin{aligned} \mathbf{f}_i &= \int_{\Omega} \mathbf{B}^T \mathbf{c} \boldsymbol{\varepsilon}_i^0 d\Omega = \int_{\Omega} \mathbf{B}^T \mathbf{c} \mathbf{B} \boldsymbol{\chi}_i^0 d\Omega = \int_{\Omega} \mathbf{B}^T \mathbf{c} \mathbf{B} d\Omega \boldsymbol{\chi}_i^0 = \mathbf{K} \boldsymbol{\chi}_i^0 \\ \bar{\mathbf{f}}_i &= \mathbf{K} \bar{\boldsymbol{\chi}}_i^0 \end{aligned} \tag{3}$$

After that, the corresponding force vectors are applied to each node in the unit cell, and the equilibrium equations in Eq. (4) under periodic boundary conditions can be solved by performing the second static analysis to obtain characteristic displacement fields (nodal displacement fields)  $\mathbf{a}_i^*$  and  $\bar{\mathbf{a}}_i^*$

$$\begin{aligned} \tilde{\mathbf{K}} \mathbf{a}_i^* &= \mathbf{f}_i \\ \tilde{\mathbf{K}} \bar{\mathbf{a}}_i^* &= \bar{\mathbf{f}}_i \end{aligned} \tag{4}$$

where  $\tilde{\mathbf{K}}$  is the stiffness matrix under periodic boundary conditions. The above characteristic displacements  $\mathbf{a}_i^*$  and  $\bar{\mathbf{a}}_i^*$  can be calculated directly by use of commercial software.

The characteristic strain fields  $\boldsymbol{\varepsilon}_i^*$  and  $\bar{\boldsymbol{\varepsilon}}_i^*$  can also be expressed by the corresponding characteristic displacement fields  $\mathbf{a}_i^*$  and  $\bar{\mathbf{a}}_i^*$  with strain–displacement matrix  $B$

$$\begin{aligned} \boldsymbol{\varepsilon}_i^* &= \mathbf{B}\mathbf{a}_i^* \\ \bar{\boldsymbol{\varepsilon}}_i^* &= \mathbf{B}\bar{\mathbf{a}}_i^* \end{aligned} \tag{5}$$

The above characteristic displacement fields  $\mathbf{a}_i^*$  and  $\bar{\mathbf{a}}_i^*$  are applied to the initial FE model, and the corresponding nodal reaction forces  $\mathbf{P}_i^*$  and  $\bar{\mathbf{P}}_i^*$  can be obtained by performing the third static analysis

$$\begin{aligned} \mathbf{K} \mathbf{a}_i^* &= \mathbf{P}_i^* \\ \mathbf{K} \bar{\mathbf{a}}_i^* &= \bar{\mathbf{P}}_i^* \end{aligned} \tag{6}$$

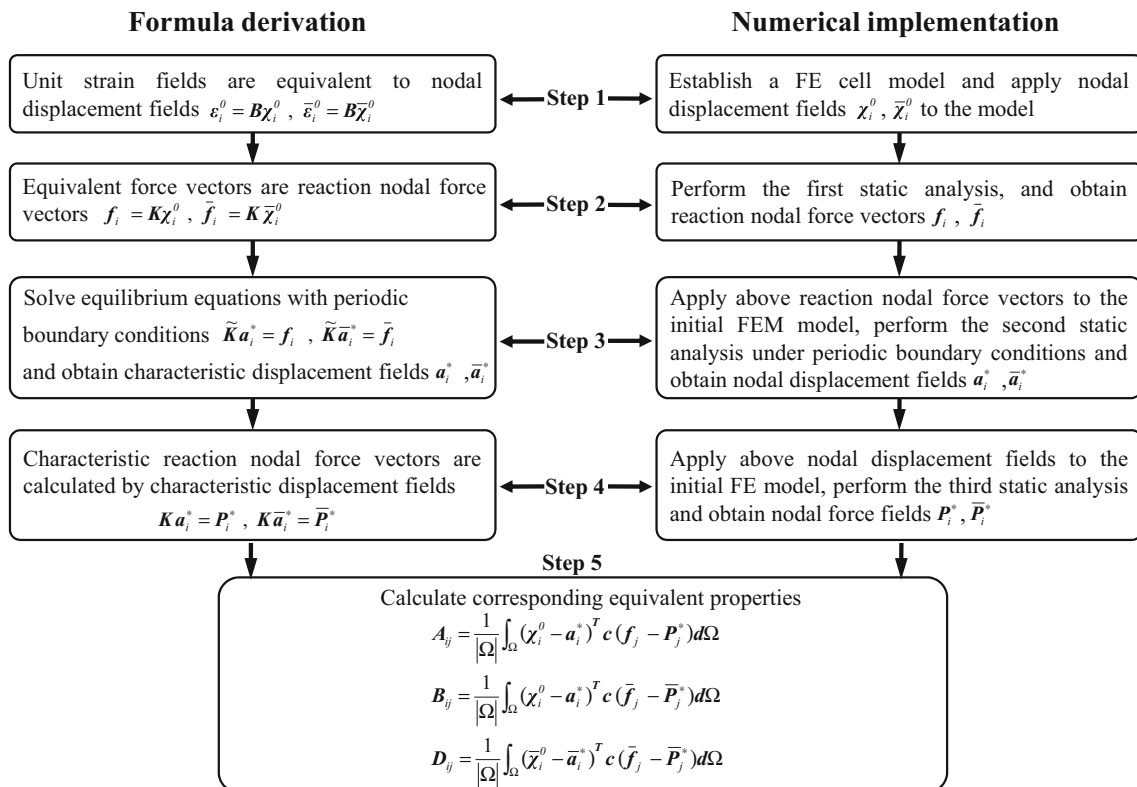


Fig. 2 Formula derivation and numerical implementation of the NIAH method

Submitting Eqs. (2, 3, 4, 5, 6) into Eq. (1), the effective stiffness coefficients of the periodic unit cell  $\Omega$  can be expressed as

$$\begin{aligned}
 \mathbf{A}_{ij} &= \frac{1}{|\Omega|} \int_{\Omega} (\chi_i^0 - \mathbf{a}_i^*)^T \mathbf{c} (\mathbf{f}_j - \mathbf{P}_j^*) d\Omega \\
 \mathbf{B}_{ij} &= \frac{1}{|\Omega|} \int_{\Omega} (\chi_i^0 - \mathbf{a}_i^*)^T \mathbf{c} (\bar{\mathbf{f}}_j - \bar{\mathbf{P}}_j^*) d\Omega \\
 \mathbf{D}_{ij} &= \frac{1}{|\Omega|} \int_{\Omega} (\bar{\chi}_i^0 - \bar{\mathbf{a}}_i^*)^T \mathbf{c} (\bar{\mathbf{f}}_j - \bar{\mathbf{P}}_j^*) d\Omega
 \end{aligned} \tag{7}$$

In this way, stiffened shell can be converted into an unstiffened shell with anisotropy property, and thus the computational cost of nonlinear post-buckling analysis can be reduced significantly. More importantly, the difference of computational cost between the equivalent model and detailed model would be much greater in the context of optimization, where hundreds of analyses are required. It should be noted that the post-buckling analysis of the equivalent unstiffened shell enable the possibility of handling the geometric nonlinearity. However, this equivalent model cannot take local buckling modes into account, thus the final optimum design should be validated by detailed model.

### 3 Fast procedure for non-uniform optimum design of stiffened shells under buckling constraint

#### 3.1 Framework of fast procedure

With regard to non-uniform axial compression, each sub-panel of stiffened shells should be designed separately to achieve a simultaneous buckling pattern and high load-carrying efficiency. However, this may result in numerous design variables and unbearable computational burden, which is a great challenge for existing optimization methodologies due to the convergence rate and computational burden (Haftka and Watson 2006; Schutte and Haftka 2010). For the gradient-based optimization methods, it is not applicable because of the discrete variables. For the Mixed-Integer Nonlinear Programming method (MINLP), the number of variables is too many, and the design domain is non-convex. More importantly, the necessary condition of global optimum is very hard to describe for the MINLP method. For this type of problems, evolutionary optimization algorithms have the potential to find the global optimum. However, once the evolutionary algorithms are employed, the computational burden is hard to afford, even if surrogate model is utilized. To this end, a fast procedure for non-uniform optimum design

of stiffened shells under buckling constraint is proposed, as shown in Fig. 3.

Since the computational cost of nonlinear post-buckling analysis is unaffordable for detailed FEA of stiffened shells, the NIAH method is utilized to smear out the stiffened sub-panels into unstiffened shells, aiming to improve the computational efficiency with only little accuracy sacrifice. It should be noted that weld lands are still treated as unstiffened thick shells, which are used to link the adjacent sub-panels. Then, the equivalent model can be constructed for post-buckling analysis. The prediction accuracy of the equivalent model should be validated before it can be utilized with full confidence.

In the previous studies, it has been demonstrated that geometric imperfections play a significant role on the variable values of the optimum design, and eigenmode-shape imperfection is a conservative choice for the prediction of knock-down effect. In particular, the presence of imperfections increases the nonlinearity of post-buckling behavior of stiffened shells, which needs to be taken into full consideration, in order to give an accurate prediction of collapse load in real working condition. Subsequently, the post-buckling analysis of stiffened shells with geometric imperfections can be performed based on the equivalent model, with a large improvement of computational efficiency but only little accuracy sacrifice.

On this basis, the emphasis is then put on the design of stiffened shells with different sub-panels. Before stiffened

shells can be optimized, the independent sub-panels should be determined firstly in terms of non-uniform load, since the optimization efficiency would be significantly reduced with the increase of the number of independent sub-panels. Therefore, it is strongly recommended that the stiffener configurations of sub-panels under the symmetric non-uniform load are imposed to be identical, for the purpose of reducing the number of independent variables. Furthermore, some symmetric sub-panels along axial direction can also be linked together.

Then, the hierarchical optimization for non-uniform optimum design of stiffened shells under buckling constraint can be carried out, which can be divided into two levels. The involved variables include stiffener type, skin thickness, stiffener height and thickness, the numbers of axial and circumferential stiffener cells. In the first level, the stiffener type and numbers of axial and circumferential stiffener cells of each independent sub-panel are optimized, in order to obtain an optimum stiffness design in the upper level. Based on the optimum design, the second-level optimization can be performed, and more detailed variables are involved, including skin thickness, stiffener height and thickness. In particular, the considered stiffener type contains of orthogrid, triangle grid, rotated triangle grid and diamond grid shapes, as shown in Fig. 4 (Wang and Abdalla 2015). Besides, from the point-of-view of easy manufacturing and economy, the stiffener height and skin thickness of each sub-panel are imposed to be equal. The effectiveness of the proposed hierarchical optimization framework would be validated through a simple benchmark example in the following section.

For the optimizations in each level, surrogate-based techniques are recommended to be used to further release the computational burden of the optimization. To ensure the feasibility of the predicted optimum design, a typical surrogate-based optimization usually consists of two loops: inner optimizations and outer updates, as shown in Fig. 5 (Queipo et al. 2005). The surrogate model is improved by sampling new points in promising areas. If the relative error between the results predicted by surrogate model and the ones from detailed FEA is less than 0.1%, the optimization is considered to be converged, otherwise, the surrogate model would be updated by the current optimum design, and then another inner optimization is performed based on the new surrogate model (Hao et al. 2016b and 2016c). For the surrogate-based optimization of stiffened shells, computational time has mainly been spent on the sampling points in design of experiment and outer updates. Once the surrogate model is constructed successfully, the optimization process only requires negligible computational cost even if genetic algorithm is employed. Finally, the detailed model of the optimum design is established, and the post-buckling analysis is performed to verify the optimum design obtained by the equivalent model. If succeed, the optimization iteration is terminated, otherwise, go back to the step of constructing the equivalent model.

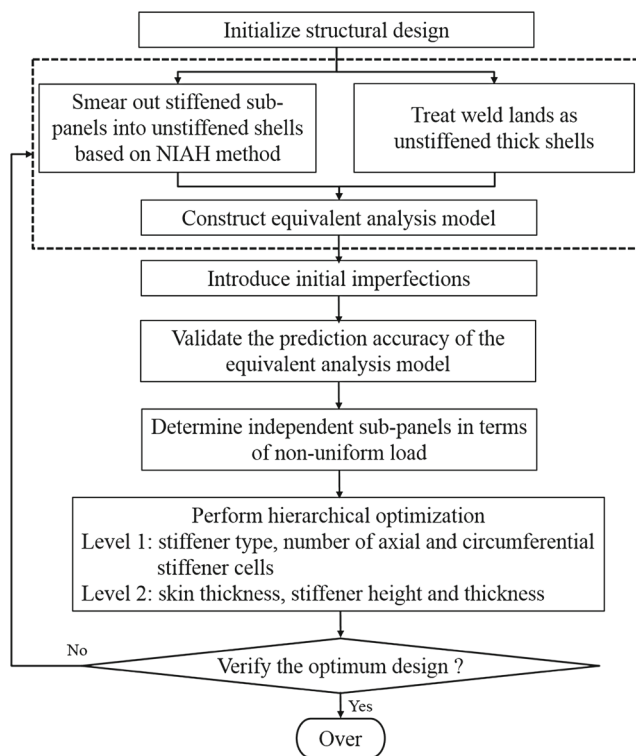
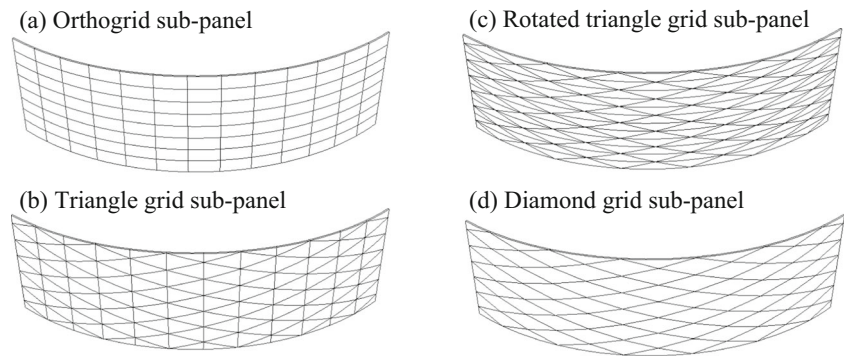


**Fig. 3** Fast procedure for non-uniform optimum design of stiffened shells under buckling constraint

**Fig. 4** Sub-panels with different stiffener types. **a** orthogrid sub-panel; **b** triangle grid sub-panel; **c** rotated triangle grid sub-panel; **d** diamond grid sub-panel



### 3.2 Validation of hierarchical optimization framework

To demonstrate the efficiency of the proposed hierarchical optimization framework, a simple benchmark example is investigated in this Section. An orthogrid stiffened shell under uniform compression is established according to the literature (Wang et al. 2014), as shown in Fig. 6. This stiffened shell is representative of the interstage of current launch vehicles, with a diameter of  $D = 3000.0$  mm, length of  $L = 2000.0$  mm. To be specific, the numbers of axial and circumferential stiffener cells  $N_a$  and  $N_c$  are 12 and 45, respectively. The skin thickness  $t_s$  is 4.0 mm. The stiffener width  $t_r$  and height  $h$  are 9.0 and 15.0 mm, respectively.

For this example, the design space of each variable is listed in Table 1. Three types of surrogate-based optimizations are performed for the purpose of comparison, where the total number of sampling points in the design of experiment are identical. Specifically, the sampling points are generated by the Optimal Latin Hypercube Sampling (OLHS) method, and then Radial basis functions (RBF) model is constructed based on the sampling data. After that, Multi-Island Genetic Algorithm (MIGA) is utilized to search for the global optimum design. The first optimization is a direct surrogate-based optimization (DSBO), where all the design variables are optimized simultaneously, and the number of sampling points is 120. The last two optimizations are hierarchical optimizations with two levels, and the number of sampling points in each level is 60. For the second optimization (referred as

hierarchical optimization I), the stiffener type  $p_1$  and the number of circumferential stiffener cells  $N_c$  and the number of axial stiffener cells  $N_a$  are involved in the first level, and the skin thickness  $t_s$ , stiffener width  $t_r$  and stiffener height  $h$  are optimized in the second level. For the third optimization (referred as hierarchical optimization II), the variables in each level are exchanged in comparison with the hierarchical optimization I. The iteration histories of three optimizations are shown in Fig. 7. It can be observed that the hierarchical optimization I is competitive in searching for the optimum design, increasing by 15.2% than the result of DSBO. By comparison with the result of hierarchical optimization II, the reasonability of the level decomposition of hierarchical optimization I is highlighted, which achieves an improvement of 9.6%. Through this benchmark example, the efficiency of the proposed hierarchical optimization framework can be validated.

## 4 Non-uniform optimum design of fuel tank in launch vehicles

### 4.1 Model description

A 1600-mm-diameter fuel tank in the booster of launch vehicles is established, as shown in Fig. 8. Differing from other previous studies (Hilburger et al. 2006; Degenhardt et al. 2008; Hao et al 2016d), the domes and internal pressure are taken into consideration. The fuel tank is composed of a

**Fig. 5** Typical framework of a surrogate-based optimization

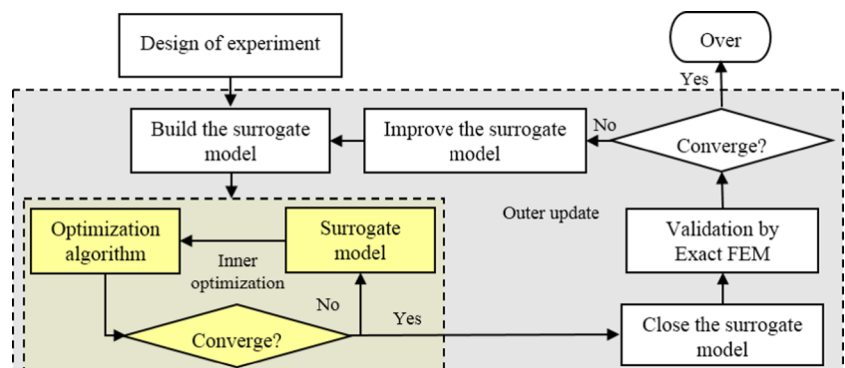
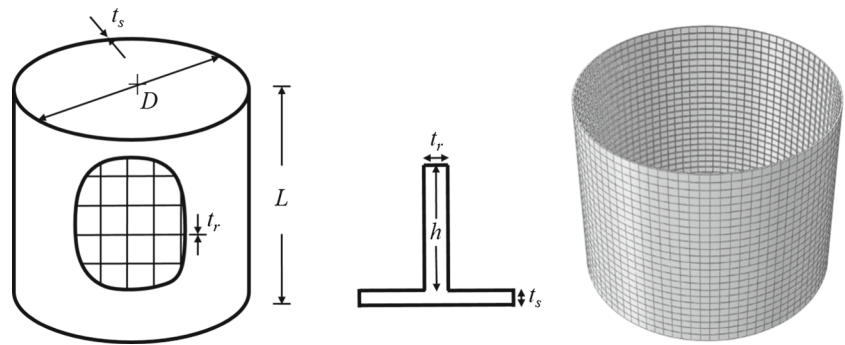


**Fig. 6** Schematic diagram of the benchmark example



welded stiffened shell, two Y-rings and two domes. In particular, the cylindrical stiffened shell can be segmented into nine sub-panels, and each sub-panel has a height of 1000 mm and a circumferential angle of 120°. Different sub-panels are manufactured separately and then welded together to form a whole stiffened shell. The upper and lower Y-rings are connected with the stiffened shell, and the upper and lower domes are attached to the Y-rings. The sub-panel is stiffened by equilateral triangle stiffeners, with a stiffener thickness of 6.0 mm, a stiffener height of 12.0 mm, a skin thickness of 4.0 mm, the numbers of axial and circumferential stiffener cells of 8 and 8. The width and thickness of weld lands are 30.0 mm and 9.0 mm, respectively. The height and thickness of Y-rings are simplified to take uniform values of 80.0 mm and 12.0 mm, respectively. The height and thickness of domes are 300.0 mm and 5.0 mm, respectively. Typical properties of the aluminum alloy used are assumed as follows: Young’s modulus  $E = 68$  GPa, Poisson’s ratio  $\nu = 0.3$ , yield stress  $\sigma_s = 410$  MPa, ultimate stress  $\sigma_b = 480$  MPa, elongation  $\delta = 0.07$ . The structural weight of the initial design is 285 kg.

To simulate the load path of booster, a rigid nose cone is also established and connected to the upper end of fuel tank, and the axial compression is loaded at the nose. Based on this model, the load distribution can vary circumferentially every time when the stiffness changes, which coincides with the true

condition of launch vehicle. The loading process is composed of internal pressure and axial compression loading processes, and the lower end of fuel tank is fully clamped. From 0 to 100 ms, increase the internal pressure linearly from zero to the maximum value 0.155 MPa. After that, from 100 to 300 ms, keeping the internal pressure as a constant status, increase the axial compression load at the nose proportionally from zero to the maximum until collapse occurs. In this case, the axial compression at the upper end of fuel tank would be non-uniform along circumferential direction. According to the symmetry of loading condition, there are six independent sub-panels in the fuel tank model. The panel number is assigned for each independent sub-panel, as shown in Fig. 8.

The finite element model is established in ABAQUS software by use of S4R shell element, which is a 4-node doubly curved general-purpose shell element with reduced integration. According to our previous works (Hao et al. 2013), the imperfection shape changes during the optimization, which is selected as the lowest mode shape of current design in each iteration. However, the maximal normalized imperfection amplitude is fixed once it is determined according to the imperfection sensitivity analysis of the initial design. This means that the absolute imperfection amplitude still changes in the optimization process with the change of skin thickness. As is evident from the imperfection sensitivity curve of the initial

**Table 1** Design space and optimum results for the benchmark example

Type	Initial design	Lower bound	Upper bound	Optimum design		
				Direct surrogate-based optimization	Hierarchical optimization I	Hierarchical optimization II
$p_1$	1	1	4	2	2	2
$t_s$ [mm]	4.0	2.5	5.5	3.1	4.2	4.1
$t_r$ [mm]	9.0	6.0	15.0	10.6	6.0	7.2
$H$ [mm]	15.0	9.0	23.0	15.0	21.4	18.2
$N_a$	12	6	18	6	7	7
$N_c$	45	25	65	52	43	44
$W$ [kg]	354	—	—	354	354	354
$P_{co}$ [kN]	16792	—	—	18190	20735	19120

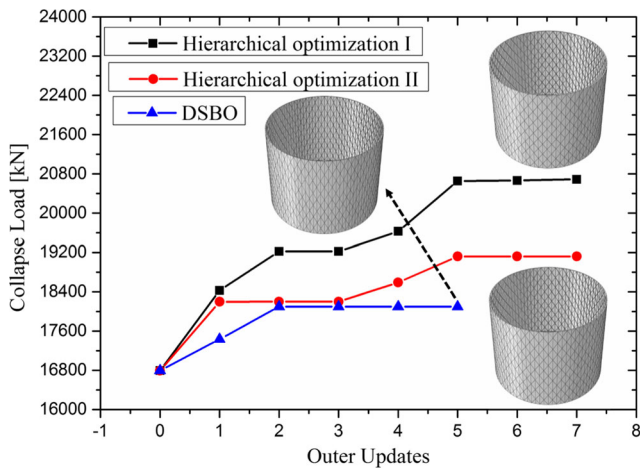


**Fig. 7** Histories of outer updates for three optimizations of the benchmark example

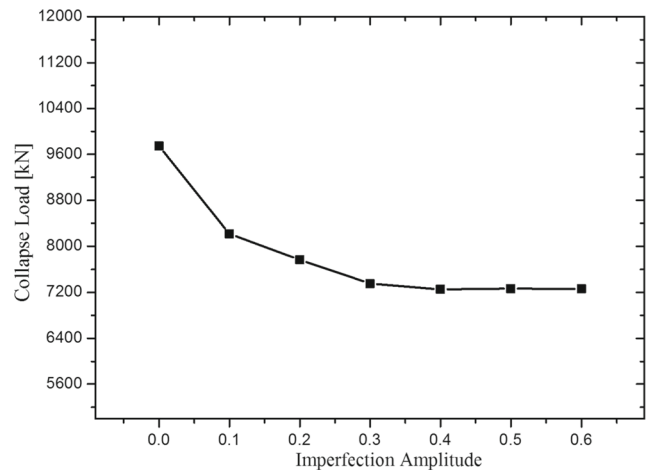


**Fig. 9** Imperfection sensitivity curve of the initial design

design shown in Fig. 9, the collapse load almost does not decrease with the increase of imperfection amplitude, when the normalized imperfection amplitude is larger than 0.3. Therefore, the normalized imperfection amplitude is selected as 0.6 (the absolute imperfection amplitude equals to 0.6 times of the skin thickness) for this example, which can reduce the influence of imperfection change during the optimization in a rational manner.

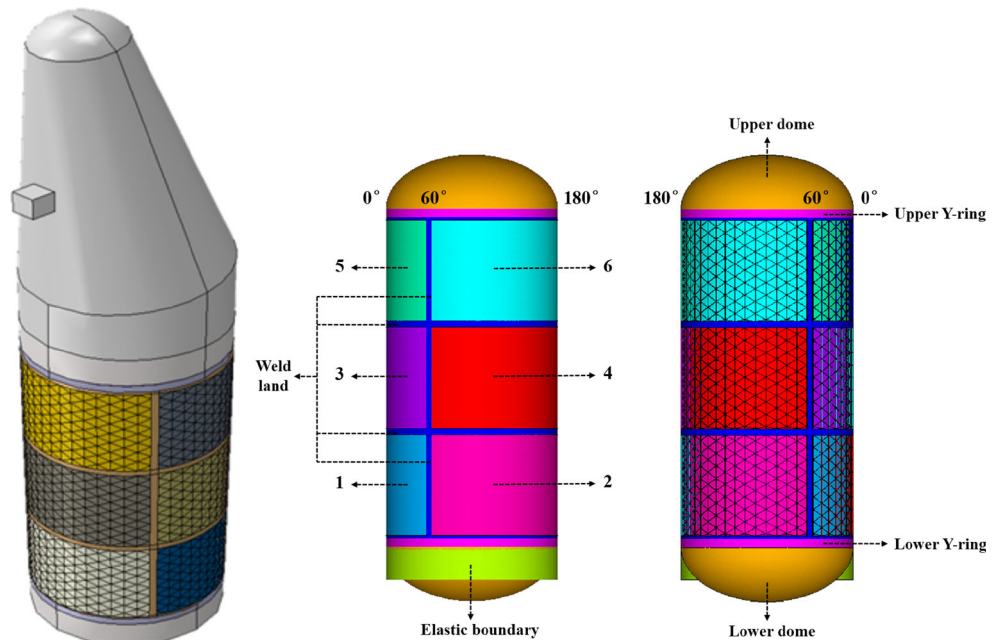
Based on the nonlinear explicit dynamic analysis, the collapse load predicted by the detailed model is 7250 kN, and the CPU time is about 1.0 h, using a work station with a CPU of Intel Xeon E5-2697 2.7 GHz and 128G RAM. The predicted load versus end-shortening curve is shown in Fig. 10, together with the deformation shape at the collapse load. To be more clear, this curve starts from the point when axial compression is applied. As is evident from Fig. 10, the buckling deformation mainly concentrates in the

sub-panel 3, which coincides with the tendency of applied axial load. In addition, it should be noted that the internal pressure has a positive effect on the axial load-carrying capacity of fuel tank.

### 4.2 Validation of equivalent analysis model

Since there are many small-size elements involved in the detailed model due to the presence of stiffeners, the computational cost of post-buckling analysis is usually very high for the detailed model. To cope with this issue, the equivalent analysis model is constructed by utilization of NIAH method. To be specific, stiffened sub-panels are smeared out into equivalent unstiffened shells, while weld lands, domes and other attachments are reserved. Since most small-size

**Fig. 8** Schematic diagram of the fuel tank





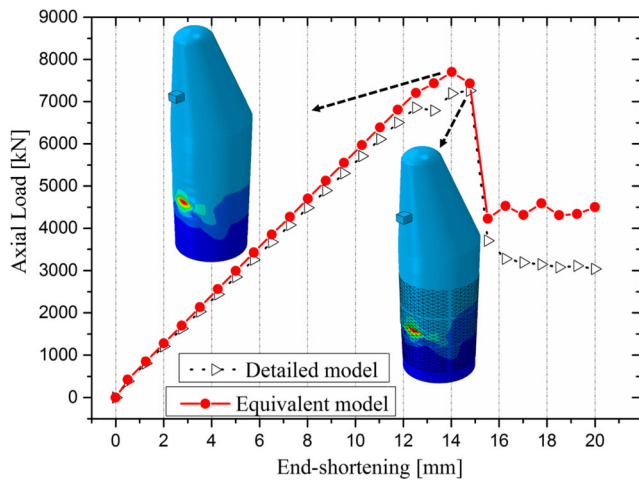


**Fig. 10** Load versus end-shortening curves of the initial design obtained by the detailed model and equivalent model

elements are eliminated, the time increment of explicit dynamic analysis can be increased to improve the computational efficiency. However, it should be noted that the equivalent model would overestimate the collapse load, once material yielding occurs before global collapse (i.e. plastic buckling), because the equivalent model cannot obtain the true stress at smeared regions due to the lack of mapping between the smeared unit cell (described by the effective stiffness coefficients) and real geometry. Fortunately, the weld lands in the equivalent model still have the true material property, thus the definition of collapse load (referred as nominal collapse load) is improved by considering the stress constraint of weld lands, rather than purely selected as the peak of load versus end-shortening curve. Specifically, the nominal collapse load is defined as the smaller axial load at the time increment when global collapse occurs and the one when material yielding of weld lands occurs. By this way, the influence of plastic buckling on the prediction error of equivalent model can be reduced.

Then, the predicted load versus end-shortening curve can also be obtained by use of equivalent model, as shown in Fig. 10. The predicted collapse load is 7703 kN, and the nominal collapse load is 7436 kN, which is closer to the one

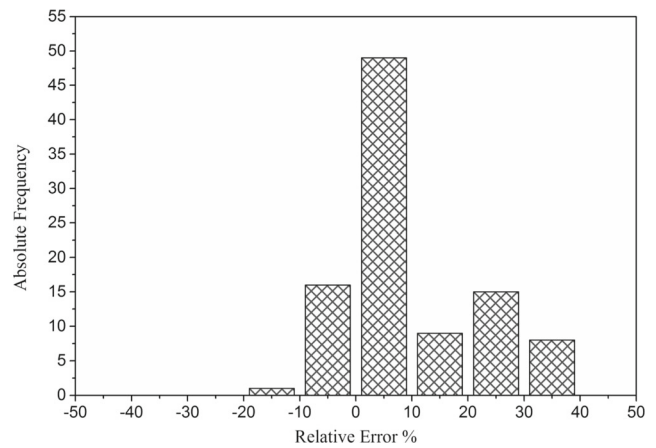


**Fig. 11** Frequency histogram of relative errors between the collapse loads predicted by the equivalent model and detailed model

obtained by the detailed model. The nominal collapse load indicates a relative error of 1.2% compared to the detailed model. Also, the tendencies of two load versus end-shortening curves agree well, especially for the deformation at the collapse load. The comparison with the detailed model reveals that the equivalent model can be confidently used to predict the post-buckling behavior of the fuel tank under non-uniform load. More importantly, the CPU time can be reduced to 0.3 h, which is only 1/3 of the one of detailed model. It can be concluded that the gain in terms of the CPU time is very significant.

Before the optimization can be performed by use of equivalent model, it should be validated by the detailed model. Therefore, a set of 100 sampling points is uniformly selected from the design space. For the illustrative example, the design spaces of each variable are specified to guarantee the rationality of each design point, as listed in Table 2, including the stiffener type  $p$ , the skin thickness  $t_s$ , the stiffener height  $h$ , the numbers of axial and circumferential stiffener cells  $N_a$  and  $N_c$ , respectively. In particular, four stiffener types are assigned with type numbers, ranging from 1 to 4. Besides,  $N_a$  and  $N_c$  are determined in terms of stiffener type. To keep a consistent representation, the nominal number of stiffener cells  $\tilde{N}_a$  and

**Table 2** Design space of variables for the fuel tank example

Type	Initial design	Lower bound	Upper bound	Stiffener type
$p_i$	2	1	4	—
$t_s$ [mm]	4.0	2.5	5.5	Arbitrary
$t_{ri}$ [mm]	6.0	3.0	9.0	Arbitrary
$h$ [mm]	12.0	8.0	16.0	Arbitrary
$N_{ai}$	—	6	16	Orthogrid
$N_{ci}$	—	13	23	Orthogrid
$N_{ai}$	8	4	14	(Rotated) triangle grid, diamond grid
$N_{ci}$	8	6	16	(Rotated) triangle grid, diamond grid

Note that the subscript  $i$  stands for the independent sub-panel number

**Table 3** Design space and optimum results for the first-level optimization of hierarchical optimization I

Type	Initial design	Lower bound	Upper bound	Hierarchical optimization I
$p_1$	2	1	4	2
$p_2$	2	1	4	1
$p_3$	2	1	4	2
$p_4$	2	1	4	2
$p_5$	2	1	4	4
$p_6$	2	1	4	1
$N_{a1}$	8	4	14	6
$N_{c1}$	8	6	16	7
$N_{a2}$	8	6	16	8
$N_{c2}$	8	13	23	17
$N_{a3}$	8	4	14	6
$N_{c3}$	8	6	16	8
$N_{a4}$	8	4	14	6
$N_{c4}$	8	6	16	6
$N_{a5}$	8	4	14	8
$N_{c5}$	8	6	16	16
$N_{a6}$	8	6	16	9
$N_{c6}$	8	13	23	23
$W$ [kg]	285	—	—	266
$P_{co}$ [kN]	7250	—	—	7345

$\tilde{N}_c$  are used in the optimization process for each stiffener type, which are in the ranges of [2, 12].

The frequency histogram of relative errors between the collapse loads predicted by the equivalent model and detailed model is shown in Fig. 11. The relative errors of equivalent model are within  $\pm 10\%$  in most situations, accounting for about 65% of the total sampling points, and the maximal

**Table 4** Design space and optimum results for the second-level optimization of hierarchical optimization I

Type	Initial design	Lower bound	Upper bound	Hierarchical optimization I
$t_s$ [mm]	4.0	2.5	5.5	3.5
$t_{r1}$ [mm]	6.0	3.0	9.0	5.5
$t_{r2}$ [mm]	6.0	3.0	9.0	3.0
$t_{r3}$ [mm]	6.0	3.0	9.0	6.3
$t_{r4}$ [mm]	6.0	3.0	9.0	3.1
$t_{r5}$ [mm]	6.0	3.0	9.0	4.8
$t_{r6}$ [mm]	6.0	3.0	9.0	3.1
$h$ [mm]	12.0	8.0	16.0	16.0
$W$ [kg]	266	—	—	240
$P_{co}$ [kN]	7345	—	—	7252

relative error is 49.0%. However, the error of equivalent model is slightly higher than the example provided in Hao et al. (2016a), because several nonlinear factors are involved in this study, including non-uniform axial load, internal pressure, material yielding and geometric imperfections. For the error sources, it can generally be attributed to two causes: periodicity and plasticity. The periodic boundary condition is not strictly satisfied for the stiffened cells with a relatively large spacing, which may cause the accuracy loss of stiffness matrix. This can be verified by the fact that the prediction accuracy of close-spaced stiffened shells is generally higher than that of stiffened shells with large spacing. On the other hand, plastic buckling is also the main source of prediction errors for equivalent model. Since the equivalent model is constructed based on the asymptotic homogenization method, the true stress field cannot be obtained at each load increment. Fortunately, a large relative error usually corresponds to a design that severely violates constraints, which would only have little impact on searching the optimum design, since the optimum design is usually near the boundary of constraints. Thus, the equivalent model can be adopted in the hierarchical optimization of stiffened shell with full confidence. By utilization of equivalent model, the total CPU time of this set of sampling points can be reduced from 159 to 48 h. This time saving represents a crucial aspect to move from a more costly optimization to a faster optimization loop.

### 4.3 Non-uniform optimum design of stiffened shells under buckling constraint

In this section, optimum designs are obtained by considering geometric imperfections in the optimization procedure. The optimization formulation can be written as

$$\begin{aligned}
 & \text{Minimize} && : W \\
 & \text{Subject to} && : P_{co} \geq P_{co0} \\
 & && \sigma_{\max} \leq \sigma_s \\
 & && X_i^l \leq X_i \leq X_i^u, i = 1, 2, \dots, n
 \end{aligned} \tag{8}$$

where  $P_{co}$  is the collapse load,  $W$  is the structural weight,  $P_{co0}$  is the collapse load of the initial design,  $\sigma_{\max}$  is the maximum stress in the weld lands,  $\sigma_s$  is the yield stress,  $X_i$  is the  $i$ th design variable, and are the lower and upper bounds of the  $i$ th design variable, as given in Table 2. According to the load condition, there are six independent sub-panels for the illustrative example.

Following the framework in Section 3, the original optimization can be substituted by a two-level optimization. In the first level, the involved variables are the numbers of axial and circumferential stiffener cells, the stiffener type of each

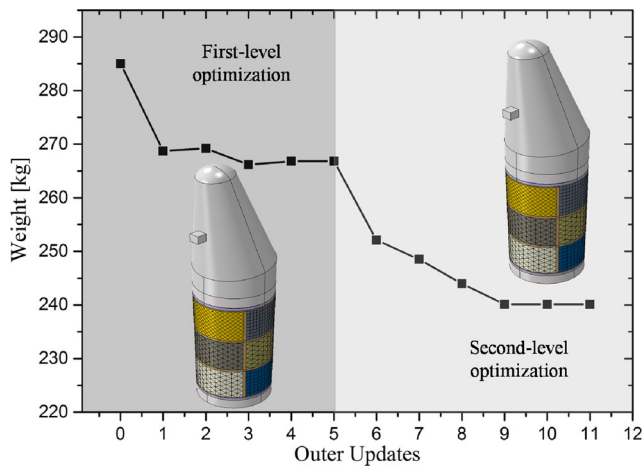


Fig. 12 Histories of the outer updates for the hierarchical optimization I

independent sub-panel. The total number of variables is 18, and the design space of each variable is listed in Tables 3. A set of 360 sampling points is generated by the OLHS method, and then RBF model is constructed based on the sampling data. After that, MIGA is utilized to search the global optimum design. To guarantee the convergence rate of optimization, detailed model is employed in the outer updates, and the stress constraint is also considered. The history of outer updates for the first-level optimization is shown in Fig. 12. The optimal values of variables for each independent sub-panel are also given in Table 3 and Fig. 12. As can be seen, the triangle grid stiffeners are used in the sub-panels under larger axial load (e.g. sub-panels 1 and 3), while the orthogrid stiffeners are employed in the ones under smaller axial load. This is due to the fact that triangle grid stiffeners can provide higher specific stiffness compared to other stiffener types. However, orthogrid stiffeners usually lead to a lower imperfection sensitivity. In addition, it should be noted that the triangle grid stiffeners are also used in the sub-panel 4, which can attract more axial load for the sub-panels near 180° and reduce the

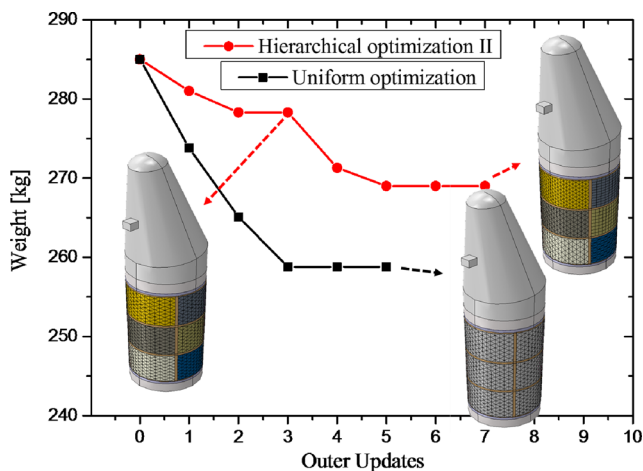


Fig. 13 Histories of the outer updates for the uniform optimization and hierarchical optimization II

Table 5 Design space and optimum results for the uniform optimization

Type	Initial design	Lower bound	Upper bound	Uniform optimization
$N_a$	8	4	14	7
$N_c$	8	6	16	9
$t_s$ [mm]	4.0	2.5	5.5	3.1
$t_r$ [mm]	6.0	3.0	9.0	5.2
$h$ [mm]	12.0	8.0	16.0	15.0
$W$ [kg]	285	—	—	260
$P_{co}$ [kN]	7250	—	—	7320

risk of buckling that occurs in the sub-panels near 0°. Due to the similar reason, the cell numbers of sub-panels 2 and 6 are relatively larger. The structural weight is reduced to 266 kg in this level, and the collapse load predicted by the detailed model is 7345 kN.

In the second level, the design variables include skin thickness, stiffener height and thickness, as listed in Table 4 and the total number of variables is 8. Similarly, a set of 160 sampling points is generated by the OLHS method, and another new RBF model is then established. The history of outer updates for the second-level optimization is also shown in Fig. 12, together with the geometry of the optimum design. The stiffener height takes a value of upper bound, while the skin thickness decreases compared to the initial design. Similar to the tendency observed in the stiffener type, the stiffener height of these sub-panels under larger axial load (e.g. sub-panels 1, 3 and 5) are significantly larger than the ones under smaller load. This can be attributed to the fact that geometric imperfections mainly occur at these regions, which may cause the reduction of load-carrying capacity. The structural weight is reduced to 240 kg in this level, and the collapse load predicted by the detailed model is 7345 kN. Finally, a weight reduction

Table 6 Design space and optimum results for the first-level optimization of hierarchical optimization II

Type	Initial design	Lower bound	Upper bound	Hierarchical optimization II
$t_s$ [mm]	4.0	2.5	5.5	3.5
$t_{r1}$ [mm]	6.0	3.0	9.0	7.0
$t_{r2}$ [mm]	6.0	3.0	9.0	5.2
$t_{r3}$ [mm]	6.0	3.0	9.0	6.0
$t_{r4}$ [mm]	6.0	3.0	9.0	6.0
$t_{r5}$ [mm]	6.0	3.0	9.0	7.5
$t_{r6}$ [mm]	6.0	3.0	9.0	4.2
$h$ [mm]	12.0	8.0	16.0	14.3
$W$ [kg]	285	—	—	278
$P_{co}$ [kN]	7250	—	—	7261

**Table 7** Design space and optimum results for the second-level optimization of hierarchical optimization II

Type	Initial design	Lower bound	Upper bound	Hierarchical optimization II
$p_1$	2	1	4	2
$p_2$	2	1	4	3
$p_3$	2	1	4	2
$p_4$	2	1	4	1
$p_5$	2	1	4	2
$p_6$	2	1	4	1
$N_{a1}$	8	4	14	5
$N_{c1}$	8	6	16	10
$N_{a2}$	8	4	14	5
$N_{c2}$	8	6	16	9
$N_{a3}$	8	4	14	6
$N_{c3}$	8	6	16	11
$N_{a4}$	8	6	16	8
$N_{c4}$	8	13	23	19
$N_{a5}$	8	4	14	8
$N_{c5}$	8	6	16	13
$N_{a6}$	8	6	16	11
$N_{c6}$	8	13	23	16
$W$ [kg]	278	—	—	269
$P_{co}$ [kN]	7261	—	—	7342

of 15.8% is achieved by the proposed hierarchical optimization, and the total CPU time is 165 h.

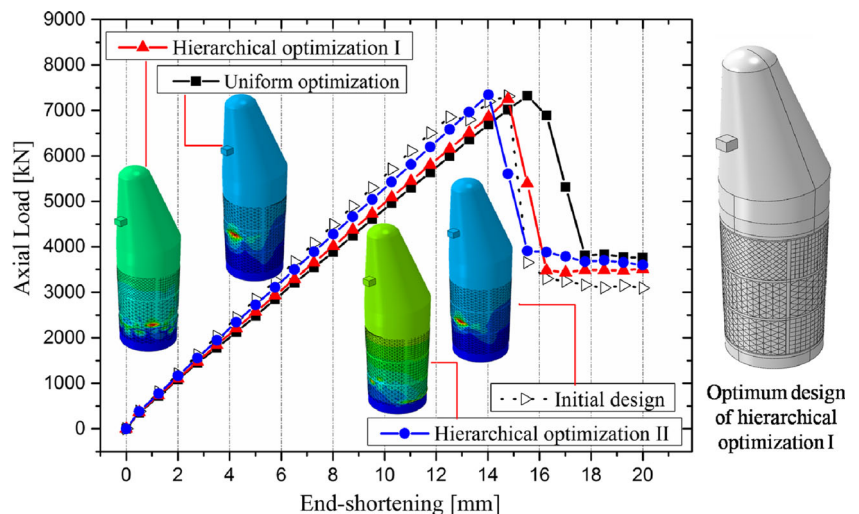
#### 4.4 Comparison with other optimization methodologies

For the purpose of comparison, uniform design optimization is performed based on the detailed model, which is representative of current design of fuel tanks in launch vehicles. To be

specific, all the design variables of each sub-panel are imposed to be identical. Thus, only five variables are involved in this optimization, including the skin thickness, stiffener height and thickness, the numbers of axial and circumferential stiffener cells. To be fair, a set of 100 sampling points is generated based on the detailed model by the OLHS method, whose CPU time is almost the same as the total CPU time of the proposed method. The history of outer updates for the uniform design optimization is shown in Fig. 13, together with the geometry of the optimum design. The variable values of the optimum design are listed in Table 5. After this optimization, only a weight reduction of 8.8% is achieved, while the total CPU time is 161 h. As expected, the current design method cannot provide variable stiffness in terms of non-uniform loads, due to the super high dimension, and thus usually leads to inefficient designs. By contrast, the proposed hierarchical optimization enhances larger design flexibility to fully explore the global load-carrying capacity, and improves the potential of weight reduction for stiffened shells.

As another important contrast, the decomposition of the design domain is then discussed. Therefore, a new optimization named as hierarchical optimization II is performed, and the variables in each level are exchanged in comparison with the hierarchical optimization I. The sampling method and size, surrogate model, optimization algorithm and convergence criterion are identical with the ones in Section 4.3. The history of outer updates for the hierarchical optimization II is also shown in Fig. 13, together with the geometry of the optimum design. The variable values of the optimum design in two levels are listed in Tables 6 and 7, respectively. The weight reductions of two levels are 7 kg and 9 kg, which are far less than the gain of the hierarchical optimization I. This is because the design space would be narrowed in an unreasonable way if the detailed variables are involved in the upper level, since they would be fixed in the lower level, which may affect the global exploration of optimum design.

**Fig. 14** Load versus end-shortening curves of three optimum designs and initial design predicted by the detailed model



Finally, the load versus end-shortening curves of three optimum designs by different optimization methods are compared in Fig. 14, together with the corresponding post-buckling patterns. As is evident, a quasi-simultaneous buckling pattern is observed for the optimum design of hierarchical optimization I, since the buckling deformation occurs at several sub-panels simultaneously, which represents a high load-carrying efficiency. By contrast, the buckling deformation mainly occurs at one or two sub-panels for other designs. Among three optimizations, the proposed fast procedure can obtain a better optimum design in an efficient manner.

## 5 Conclusions

For tailoring the non-uniform axial compression, a concept of non-uniform stiffened shell is fully utilized to enhance the potential of weight reduction, whose independent sub-panels can be determined in terms of load symmetry and then designed separately. With regard to the numerous design variables and high computational cost of post-buckling analysis, an efficient equivalent analysis model is developed based on the NIAH method. By utilization of the equivalent model, the CPU time of a typical post-buckling analysis can be reduced to 1/3 of the one by detailed model. The utilization of equivalent model into post-buckling regime is validated when non-uniform load, internal pressure and geometric imperfections are considered together. The results of 100 sampling points selected from the whole design space reveal that the equivalent model can be confidently used to predict the collapse load of fuel tanks in the post-buckling optimization.

Moreover, a fast procedure for the minimum weight design of non-uniform stiffened shells under buckling constraint is proposed, in which the hyper multi-dimensional problem is decomposed into a hierarchical optimization with two levels. The effectiveness of the decomposition of the design domain is verified by a simple benchmark example.

Finally, a typical fuel tank of launch vehicle is utilized to demonstrate the efficiency of the proposed fast procedure, and detailed comparison with several other existing methodologies is made. Results indicate that the fast procedure can provide a larger weight reduction in an efficient manner. Moreover, it should be emphasized that non-uniform stiffened shells are very convenient for current manufacturing technology, which are expected to be utilized in future launch vehicles.

**Acknowledgments** This work was supported by the National Basic Research Program of China (2014CB049000 and 2014CB046596), the National Natural Science Foundation of China (11402049 and 11372062), the Project funded by China Postdoctoral Science Foundation (2014M551070 and 2015T80246).

## References

- Azarboni HR, Darvizeh M, Darvizeh A, Ansari R (2015) Nonlinear dynamic buckling of imperfect rectangular plates with different boundary conditions subjected to various pulse functions using the Galerkin method. *Thin-Walled Struct* 94:577–584
- Bushnell D, Bushnell WD (1994) Minimum-weight design of a stiffened panel via PANDA2 and evaluation of the optimized panel via STAGS. *Comput Struct* 50(4):569–602
- Cai YW, Xu L, Cheng GD (2014) Novel numerical implementation of asymptotic homogenization method for periodic plate structures. *Int J Solids Struct* 51(1):284–292
- Carrera E, Mannella L, Augello G, Gualtieri N (2003) A two-level optimization feature for the design of aerospace structures. *Proc IME G J Aero Eng* 217(4):189–206
- Castro SGP, Zimmermann R, Arbelo MA, Khakimova R, Hilburger MW, Degenhardt R (2014) Geometric imperfections and lower-bound methods used to calculate knock-down factors for axially compressed composite cylindrical shells. *Thin-Walled Struct* 74:118–132
- Cheng GD, Cai YW, Xu L (2013) Novel implementation of homogenization method to predict effective properties of periodic materials. *Acta Mech Sinica* 29(4):550–556
- Degenhardt R, Kling A, Rohwer K, Orifici AC, Thomsonc RS (2008) Design and analysis of stiffened composite panels including post-buckling and collapse. *Comput Struct* 86(9):919–929
- Degenhardt R, Castro SGP, Arbelo MA, Zimmermann R, Khakimova R, Kling A (2014) Future structural stability design for composite space and airframe structures. *Thin-Walled Struct* 81:29–38
- Elishakoff I, Kriegesmann B, Rolfes R, Hühne C, Kling A (2012) Optimization and antioptimization of buckling load for composite cylindrical shells under uncertainties. *AIAA J* 50(7):1513–1524
- Forys P (2015) Optimization of cylindrical shells stiffened by rings under external pressure including their post-buckling behaviour. *Thin-Walled Struct* 95:231–243
- Friedrich L, Loosen S, Liang K, Ruess M, Bisagni C, Schröder K (2015) Stacking sequence influence on imperfection sensitivity of cylindrical composite shells under axial compression. *Compos Struct* 134:750–761
- Fukunaga H, Vanderplaats GN (1991) Stiffness optimization of orthotropic laminated composites using lamination parameters. *AIAA J* 29(4):641–646
- Godoy LA, Jaca RC, Sosa EM, Flores FG (2015) A penalty approach to obtain lower bound buckling loads for imperfection-sensitive shells. *Thin-Walled Struct* 95:183–195
- Greenberg JB, Stavsky Y (1995) Buckling of composite orthotropic cylindrical shells under non-uniform axial loads. *Compos Struct* 30(4):399–406
- Haftka RT, Watson LT (2006) Decomposition theory for multidisciplinary design optimization problems with mixed integer quasiseparable subsystems. *Optim Eng* 7(2):135–149
- Hao P, Wang B, Li G (2012) Surrogate-based optimum design for stiffened shells with adaptive sampling. *AIAA J* 50(11):2389–2407
- Hao P, Wang B, Li G, Tian K, Du KF, Wang XJ, Tang XH (2013) Surrogate-based optimization of stiffened shells including load-carrying capacity and imperfection sensitivity. *Thin-Walled Struct* 72(15):164–174
- Hao P, Wang B, Li G, Meng Z, Tian K, Tang XH (2014) Hybrid optimization of hierarchical stiffened shells based on smeared stiffener method and finite element method. *Thin-Walled Struct* 82(9):46–54
- Hao P, Wang B, Tian K, Du KF, Zhang X (2015a) Influence of imperfection distributions for cylindrical stiffened shells with weld lands. *Thin-Walled Struct* 93(8):177–187
- Hao P, Wang B, Li G, Meng Z, Wang LP (2015b) Hybrid framework for reliability-based design optimization of imperfect stiffened shells. *AIAA J* 53(10):2878–2889

- Hao P, Wang B, Tian K, Li G, Du KF, Niu F (2016a) Efficient optimization of cylindrical stiffened shells with reinforced cutouts by curvilinear stiffeners. *AIAA J* 54(4):1350–1363
- Hao P, Wang B, Tian K, Li G (2016b) Integrated optimization of hybrid-stiffness stiffened shells based on sub-panel elements. *Thin-Walled Struct* 103:171–182
- Hao P, Wang B, Tian K, Li G, Zhang X (2016c) Optimization of curvilinearly stiffened panels with single cutout concerning the collapse load. *Int J Struct Stab Dy* 16: 1550036-1-1550036-21
- Hao P, Wang B, Du KF, Li G, Tian K, Sun Y, Ma YL (2016d) Imperfection-insensitive design of stiffened conical shells based on perturbation load approach. *Compos Struct* 136:405–413
- Henrichsen SR, Lindgaard E, Lund E (2015) Robust buckling optimization of laminated composite structures using discrete material optimization considering “worst” shape imperfections. *Thin-Walled Struct* 94:624–635
- Hilburger MW, Nemeth MP, Starnes JH Jr (2006) Shell buckling design criteria based on manufacturing imperfection signatures. *AIAA J* 44(3):654–663
- Kalamkarov AL, Andrianov IV, Danishevsá VV (2009) Asymptotic homogenization of composite materials and structures. *Appl Mech Rev* 62(3): 030802-1-030802-20
- Lamberti L, Venkataraman S, Haftka RT, Johnson TF (2003) Preliminary design optimization of stiffened panels using approximate analysis models. *Int J Numer Methods Eng* 57(10):1351–1380
- Liang K, Zhang YJ, Sun Q, Ruess M (2015) A new robust design for imperfection sensitive stiffened cylinders used in aerospace engineering. *Sci China* 58(5):796–802
- Loughlan J (1994) The buckling performance of composite stiffened panel structures subjected to combined in-plane compression and shear loading. *Compos Struct* 29(2):197–212
- Meziane MAA, Abdelaziz HH, Tounsi A (2014) An efficient and simple refined theory for buckling and free vibration of exponentially graded sandwich plates under various boundary conditions. *J Sandw Struct Mater* 16(3):293–318
- Ovesy HR, Fazilati J (2014) Parametric instability analysis of laminated composite curved shells subjected to non-uniform in-plane load. *Compos Struct* 108:449–455
- Paulo RMF, Teixeira-Dias F, Valente RAF (2013) Numerical simulation of aluminium stiffened panels subjected to axial compression: Sensitivity analyses to initial geometrical imperfections and material properties. *Thin-Walled Struct* 62:65–74
- Peeters DMJ, Hesse S, Abdalla MM (2015) Stacking sequence optimisation of variable stiffness laminates with manufacturing constraints. *Compos Struct* 125:596–604
- Queipo NV, Haftka RT, Shyy W, Goel T, Vaidyanathan R, Tucker PK (2005) Surrogate-based analysis and optimization. *Prog Aerosp Sci* 41(1):1–28
- Ragon SA, Haftka RT, Tzong TJ (1997) Global/local Structural Wing Design using Response Surface Techniques, 38th AIAA/ASME/ASCE/AHS/ASC Structures, Structural Dynamics and Materials Conf. AIAA-1997-1051, Kissimmee, FL, April 1997
- Schutte JF, Haftka RT (2010) Global structural optimization of a stepped cantilever beam using quasi-separable decomposition. *Eng Optim* 42(4):347–367
- Soni G, Singh R, Mitra M (2013) Buckling behavior of composite laminates (with and without cutouts) subjected to nonuniform in-plane loads. *Int J Struct Stab Dyn* 13(08):1350044
- Starnes JH Jr, Haftka RT (1979) Preliminary design of composite wings for buckling, strength, and displacement constraints. *AIAA J* 16(8): 564–570
- Teng JG, Song CY (2001) Numerical models for nonlinear analysis of elastic shells with eigenmode-affine imperfections. *Int J Solids Struct* 38(18):3263–3280
- Vescovini R, Bisagni C (2013) Two-step procedure for fast post-buckling analysis of composite stiffened panels. *Comput Struct* 128:38–47
- Vitali R, Haftka RT, Sankar BV (2002) Multi-fidelity design of stiffened composite panel with a crack. *Struct Multidiscip Optim* 23(5):347–356
- Wang D, Abdalla MM (2015) Global and local buckling analysis of grid-stiffened composite panels. *Compos Struct* 119:767–776
- Wang H, Croll JGA (2015) Plateau lower-bounds to the imperfection sensitive buckling of composite shells. *Compos Struct* 133:979–985
- Wang B, Hao P, Li G, Wang XJ, Tang XH, Luan Y (2014) Generatrix shape optimization of stiffened shells for low imperfection sensitivity. *Sci China* 57(10):2012–2019
- Wang B, Tian K, Hao P, Cai YW, Li YW, Sun Y (2015) Hybrid analysis and optimization of hierarchical stiffened plates based on asymptotic homogenization method. *Compos Struct* 132(11):136–147